

First identification of a doublet wobbling excitation mode in ^{105}Pd

A. Karmakar^{1,2}, P. Datta³, N. Rather⁴, S. Pal,⁵ R. Palit,⁵ A. Goswami,^{1,#} G.H. Bhat,⁶ J. A. Sheikh,^{4,7} S. Jehangir⁴, S. Chattopadhyay^{1,2,*} and S. Frauendorf,⁸

¹*Saha Institute of Nuclear Physics, 1/AF, Bidhan Nagar, Kolkata - 700 064, India*

²*Homi Bhabha National Institute, Training School Complex, Anushakti Nagar, Mumbai - 400 094, India*

³*Ananda Mohan College, Kolkata - 700 009, India*

⁴*Department of Physics, Islamic University of Science and Technology, Awantipora, 192 122, India*

⁵*Tata Institute of Fundamental Research, Mumbai- 400005, India*

⁶*Department of Physics, GDC Shopian, Jammu and Kashmir, 192 303, India*

⁷*Department of Physics, University of Kashmir, Srinagar, 190 006, India*

⁸*Department of Physics, University of Notre Dame, Notre Dame, Indiana 46556, USA and*

Deceased

(Dated: March 14, 2024)

An experimental investigation of ^{105}Pd has revealed, for the first time, the existence of two wobbling bands both having one phonon configuration and originating from the coupling of the wobbling phonon to the ground state band and to its signature partner. The doublet one-phonon wobbling bands are, in turn, found to be the signature partner bands. These observations have been drawn from the measured ratios of the inter-band and intra-band gamma transition rates. The model calculations based on the triaxial projected shell model (TPSM) approach have been performed and are found to be in good agreement with the experimental observations. These calculations provide an insight into the nature of the observed structures at a microscopic level.

I. INTRODUCTION

The existence of triaxial deformed nuclei has been predicted by numerous mean-field studies (see e.g. Ref. [1]) for an early systematic exploration of the nuclear chart). A special feature of triaxial nuclei is that they can exhibit the wobbling motion near the yrast line and was predicted by Bohr and Mottelson in 1975 [2]. For large angular-momenta, the energy spectrum will have a harmonic oscillator pattern [2] with the bands characterized in terms of the signature quantum number. For these bands, the moments of inertia along the three principal axes are unequal and the total angular momentum (vector sum of particle and rotational angular momentum) wobbles about the medium (m) axis, which has the largest moment of inertia. The nuclear wobbling is observed as consecutive rotational bands with increasing excitation energy, corresponding to successive wobbling quanta ($\propto n\hbar\omega_W$ for large I).

Wobbling mode was originally predicted for an even-even system, however, this special high-spin mode as discussed by Bohr and Mottelson has not been observed yet. Instead, the first observation of wobbling was reported in 2001 for the odd-mass ^{163}Lu [3]. The authors interpreted their data in the framework of the particle + triaxial rotor (PTR) model (see e.g. Ref. [2]). Two bands, labelled as TSD1 and TSD2, were identified, which were associated with the triaxial strongly deformed (TSD) minimum with odd-proton occupying the $i_{13/2}$ configuration, obtained in the ultimate cranking calculations of Ref. [4]. The lower TSD1 band corresponds to $n = 0$ and the excited TSD2 band to the $n = 1$ wobbling excitation. The

presence of the high- j proton significantly modifies the wobbling motion. Using the PTR model, Frauendorf and Dönau [5] classified the collective mode into longitudinal wobbling (LW) when the angular momentum vector precesses about the medium axis of the triaxial nuclear shape and transverse wobbling (TW) when it precesses around an axis transverse to the medium axis. For increasing angular momentum, the excitation energy of the wobbling quanta increases for LW, and decreases for TW up to a critical value I_c , above which the TW changes into the LW regime. The wobbling mode represents a periodic motion of the three principal axes of the triaxial charge distribution, which generates strong E2 radiation. This is observed as collectively enhanced $\Delta I = 1$ E2 transitions between the levels of two consecutive wobbling bands. Recently, TW mode has been reported in several odd- A nuclei [3, 6–18].

The TW regime appears when the angular momentum \mathbf{j} of the odd particle aligns with the short or long axis of the nucleus which is transverse to the medium axis and for the reported cases it is the short axis. Of course, the particle alignment is not rigid and there are excitations which correspond to the reorientation of the odd particle's angular momentum \mathbf{j} , such that it precesses about the short axis with the projection $j - 1$. The bands based on this configuration have been referred to as signature partner (SP) bands [6] because it is their traditional nomenclature in high-spin physics, where the rotational bands group into $\Delta I = 2$ signature sequences connected by strong intra-band E2 transitions. (The signature of the band is defined by $\alpha = I + \text{even number}$.) In contrast to the TW bands, SP bands are connected by $\Delta I = 1$ M1 transitions with the $n = 0$ band. In all the reported cases [3, 6–18], the SP band has been observed. Both the TW and signature partner bands have the signature, $-\alpha$,

* sukalyan.chattopadhyay@saha.ac.in

that is opposite to the signature α of the $n=0$ band. The appearance of the collective TW band, in addition to the signature partner band, represents stringent evidence for triaxial deformation.

If the two distinct modes keep their dominant character, the next bands with signature α are expected to be the double TW band ($n = 2$), the TW based on the SP band and the particle excitation, where \mathbf{j} precesses about the short axis with the projection $j - 2$. The authors of Ref. [16] discussed the small amplitude limit of the particle triaxial rotor system, where the TW and SP modes appear as normal vibrational modes, which combine in an additive way.

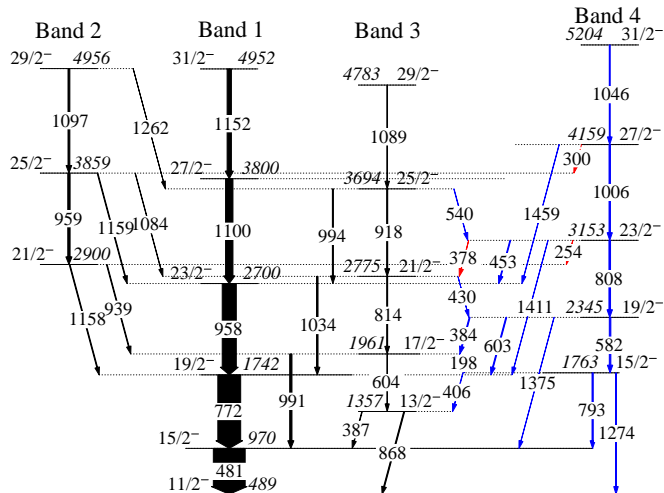


FIG. 1. The partial level scheme of ^{105}Pd established from the present work. The levels and transitions marked in Black were reported in [18] while those marked in Blue were reported [19] by the same group. Our data confirms all these levels and transitions and we have added three more transitions, which are marked in red. The spin and parities of Band 2 have been adapted from Ref. [18]

In the case of ^{135}Pr the odd particle is an $h_{11/2}$ proton and accordingly, the $n = 0$ yrast band has $\alpha = -1/2$. The TW and SP bands with $\alpha = 1/2$ were identified in Ref. [6]. The authors of Ref. [17] demonstrated that a fourth band with $\alpha = -1/2$ has the characteristics of the double TW excitation. The present case study of ^{105}Pd has a structure that is analogous to ^{135}Pr with the odd proton replaced by the odd $h_{11/2}$ neutron. The authors of Ref. [18] identified the $\alpha = -1/2$ yrast band (Band 1) and the $\alpha = 1/2$ TW (Band 3) and SP (Band 2) bands depicted in Fig. 1. This work also observed, at a somewhat larger energy, an $\alpha = -1/2$ band [19] and the authors speculated that it might be the double TW band by analogy to ^{135}Pr . However, they left the nature of the band an open problem because their data did not allow them to establish such an assignment. Through the detailed measurements of the mixing ratios of the transition connecting this band with the TW band, the present Letter provides the experimental data for a struc-

tural assignment. As will be elucidated below, the second $\alpha = 1/2$ band is not the double TW band as speculated, but is the first known example of a TW-on-SP band.

II. EXPERIMENTAL RESULTS

The high-spin states of ^{105}Pd were populated through the fusion-evaporation reaction, where the 63 MeV ^{13}C beam delivered by the 14-UD Pelletron at the Tata Institute of Fundamental Research (TIFR) was used to bombard a 1 mg/cm² enriched ^{96}Zr target with Pb backing of 9 mg/cm² thickness. The de-exciting γ rays were detected by using the Indian National Gamma Array (INGA) [20]. During the time of the experiment, the array consisted of 18 Compton-suppressed clover detectors arranged in six rings with three at 40°, two at 65°, four at 90°, three at 115°, three at 140° and three at 157° with respect to the beam direction. The two and higher-fold coincidence data were recorded by a fast-digital data acquisition system based on Pixie-16 modules [20]. The corresponding time-stamped data were sorted in a γ - γ symmetric matrix using the multiparameter time-stamped-based coincidence search (MARCOS) program, developed at TIFR [20]. The matrix was used to establish the low-lying negative parity levels of ^{105}Pd with the help of the RADWARE program LEVIT8R [21]. The partial level scheme of ^{105}Pd has been shown in Fig. 1, where the widths of the transitions are proportional to their relative intensities. The newly placed 254 keV ($23/2^- \rightarrow 21/2^-$) and 300 keV ($27/2^- \rightarrow 25/2^-$) transitions between Band 4 and Band 2 are shown in the coincidence spectrum with their respective top transitions, in Fig. 2. The relative intensities of the gamma transitions obtained from the present data agree well with the evaluated intensities from Ref. [22]. However, the intensities of the newly observed gamma transitions in Ref. [18] and [19] were not reported. These have been evaluated from the present data and tabulated in Table I.

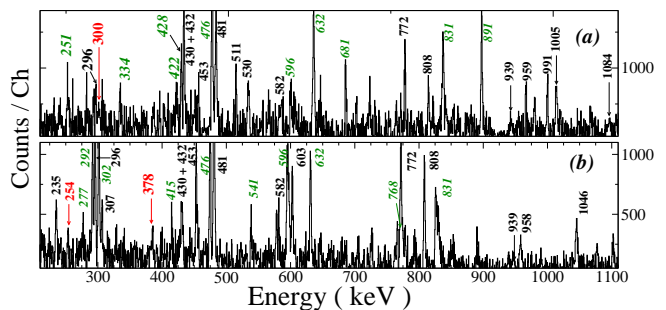


FIG. 2. The gamma spectra in coincidence with (a) 1046 keV ($31/2^- \rightarrow 27/2^-$) keV and (b) 1006 ($27/2^- \rightarrow 23/2^-$) keV transitions of Band 4. The newly placed gamma transitions from Band 4 to Band 2 have been marked in red. The transitions marked in green belong to ^{102}Ru . This contamination is due to the presence of 1047 keV ($15^- \rightarrow 13^-$) and 1005 keV ($14^- \rightarrow 12^-$) transitions in ^{102}Ru .

TABLE I. Energies, relative intensities, DCO ratios using the detectors at 40° and 157° ring along with the detectors at 90° ring, linear polarizations, mixing ratios and deduced multiplicities of transitions of ^{105}Pd shown in Fig. 1.

| E_γ (keV) | I_γ (rel.) (keV) | R_{DCO} (40°) | R_{DCO} (157°) | P | δ | Mult. |
|---------------------|----------------------------|------------------------------------|-------------------------------------|-----------|----------|-------|
| 772 | 47.93(22) | 1.04(2) | - | 0.59(3) | 0.1(4) | E2 |
| 958 | 29.51(29) | 0.98(2) | - | 0.46(4) | 0.05(4) | E2 |
| 939 | 1.01(10) | 0.96(10) | - | 1.15(64) | 0.0(1) | E2 |
| 1158 | 1.08(17) | - | 0.65(10) | - | - | M1 |
| 604 | 0.64(11) | 0.97(6) | - | - | 0.05(9) | E2 |
| 991 | 4.75(16) | 1.20(3) | 1.27(5) | -0.43(27) | 1.8(3) | Mixed |
| 198 | 0.42(11) | 0.60(24) | - | - | 0.02(15) | M1 |
| 582 | 32.75(br) | 1.06(7) | - | 0.34(27) | 0.1(1) | E2 |
| 1375 | 0.51(34) | 1.09(11) | - | - | 0.10(10) | E2 |
| 603 | 1.93(31) | 0.84(4) | 0.78(11) | -0.37(14) | -0.60(5) | Mixed |
| 384 | 19.97(br) | 0.66(5) | - | - | 0.11(4) | M1 |
| 814 | 1.98(27) | 0.98(5) | - | 0.56(45) | 0.0(5) | E2 |
| 1034 | 3.11(16) | 1.12(6) | 1.15(11) | -0.33(16) | 2.2(5) | Mixed |
| 430 | 0.28(6) | 0.65(7) | - | - | 0.08(7) | M1 |
| 808 | 3.31(27) | 0.96(6) | - | 0.33(27) | -0.1(1) | E2 |
| 1411 | 0.51(32) | 0.98(14) | - | - | 0.0(1) | E2 |
| 453 | 1.69(35) | 0.84(5) | 0.83(12) | - | -0.62(6) | Mixed |
| 378 | 1.04(23) | 0.61(13) | - | - | 0.03(13) | M1 |
| 254 | 0.27(9) | 0.94(7) | 0.97(15) | - | 0.35(7) | Mixed |
| 918 | 2.18(29) | 1.00(5) | - | 0.69(50) | 0.0(1) | E2 |
| 994 | 2.16(15) | 1.08(5) | 1.23(12) | -0.35(21) | 2.4(7) | Mixed |
| 540 | 0.66(24) | 0.65(8) | - | - | 0.07(7) | M1 |
| 1100 | 15.48(47) | 0.99(3) | - | 0.18(8) | 0.1(4) | E2 |
| 959 | 1.29(34) | - | - | - | - | - |
| 1084 | 0.48(16) | 1.03(15) | - | 0.89(74) | 0.1(1) | E2 |
| 1159 | 0.43(17) | - | - | - | - | - |
| 1006 | 2.90(48) | 1.05(9) | - | 0.75(34) | 0.1(7) | E2 |
| 1459 | 0.60(35) | 0.98(13) | - | - | 0.0(15) | E2 |
| 300 | 0.12(6) | 0.89(13) | 0.85(20) | - | 0.29(13) | Mixed |
| 1089 | 1.38(32) | 1.05(7) | - | 0.89(45) | 0.1(8) | E2 |
| 1152 | 8.96(91) | 1.00(3) | - | 0.25(17) | 0.0(5) | E2 |
| 1097 | 1.25(33) | - | - | - | - | - |
| 1262 | 0.18(9) | - | - | - | - | - |
| 1046 | 1.93(41) | 1.03(6) | - | 0.64(43) | 0.1(6) | E2 |

The γ - ray multiplicities were determined from the Ratio of Directional Correlations from Oriented states (R_{DCO}) method [23]. For this measurement, an asymmetric matrix was constructed with the γ - ray energy detected at 90° along one axis while the coincident γ - ray energy at 40° and 140° on the other axis. For the mixed transitions, the measured R_{DCO} values have been validated by re-measuring the value using the “ 157° ” and “ 90° ” matrix. For the R_{DCO} measurements, the stretched E2 gating transitions were used. The value for the attenuation coefficient of complete alignment (σ/J) of 0.31(3) was estimated from the measured R_{DCO} values for 1100 keV E2 and 1331 keV E1 transitions, which were assumed to be pure stretched transitions. The R_{DCO} values for 40° (157°) were calculated using the computer code ANGCOR [24] (for $\sigma/J = 0.31(3)$) and were found to be 1.0 and 0.58 (1.0 and 0.51) for pure $\Delta I = 2$ and $\Delta I = 1$ transitions, respectively. The linear polarization (P)

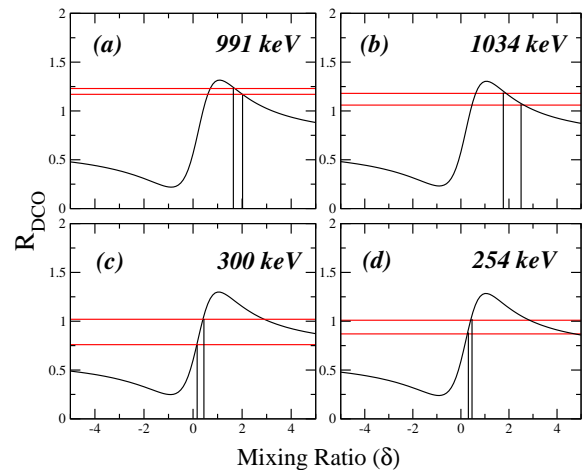


FIG. 3. Variation of the calculated R_{DCO} as a function of mixing ratio (δ) for the $\Delta I = 1$ transitions from Band 3 to Band 1 ((a) 991, (b) 1034 keV) and from Band 4 to Band 2 ((c) 300, (d) 254 keV). The horizontal lines correspond to the R_{DCO} values at 40° along with their uncertainties.

measurements were also performed to extract the electromagnetic character of the de-exciting γ rays. The results obtained from the present measurements are tabulated in Table I and are found to be consistent with previously known spin and parity assignments [18, 19]. It may be observed from Table. I that the experimental R_{DCO} values show a significant departure from the calculated values for the $\Delta I = 1$ transitions between Band 3 \rightarrow Band 1 and Band 4 \rightarrow Band 2 and also for the $\Delta I = 0$ transitions between Band 4 \rightarrow Band 1. Only these transitions (labelled as mixed in Table. I) have substantial M1/E2 mixing. The mixing ratios (δ) of 991 ($E_x = 1961$ keV), 603 ($E_x = 2345$ keV), 1034 ($E_x = 2775$ keV) and 994 ($E_x = 3694$ keV) keV transitions have been unambiguously determined through the combined measurement of R_{DCO} and P. The mixing ratios for the 991, 1034 and 994 keV transitions between the wobbling bands were reported to be 1.8(5), 2.3(3) and 2.7(6), respectively [18]. The values obtained from the present measurements are 1.8(3), 2.2(5) and 2.4(7) respectively, which are in good agreement with the previous measurements. However, for the low energy transitions of 254, 453 ($E_x = 3153$ keV) and 300 keV ($E_x = 4159$ keV), the P measurements were not possible due to inadequate statistics. In this case, the mixing ratios have been estimated by comparing the experimental R_{DCO} value with the corresponding calculated values for the different values of δ using $\sigma/J = 0.31(3)$. These plots for the two $\Delta I = 1$ transitions from Band 3 to Band 1 namely, 991 and 1034 keV and two of 254 and 300 keV from Band 4 to Band 2, are shown in Fig. 3. For Band 3 \rightarrow 1 transitions, the higher evaluated value of δ is consistent with the values obtained from the combined measurement of R_{DCO} and P. For 254 and 300 keV transitions, the estimated δ values are 0.35(7) and 0.29(13), respectively. The DCO ratios for all the observed $\Delta I = 1$ transitions between Band 3 and 4 agree

well with the calculated value for a pure dipole transition. This was also found to be true for the 1158 keV transition from Band 2 ($E_x = 2900$ keV) to Band 1. Thus, for these transitions, the E2 mixing has been found to be negligible (E2 fraction $\leq 0.1\%$). It is worth mentioning that the $17/2^-$, $21/2^-$ and $25/2^-$ levels of Band 3 decay by two $\Delta I = 1$ transitions to Band 1 and Band 4. For the three transitions to Band 1, the E2 fraction ($\frac{\delta^2}{1+\delta^2}$) is $\approx 85\%$, while for the transitions to Band 4, the E2 fraction is $\leq 0.1\%$ as obtained from Table I. It may also be noted that the E2 fraction is $\approx 10\%$ for the 254 and 300 keV transitions from Band 4 to Band 2, but the lower transition energies lead to large electric quadrupole transition rates ($B(E2)$) for these $\Delta I = 1$ transitions.

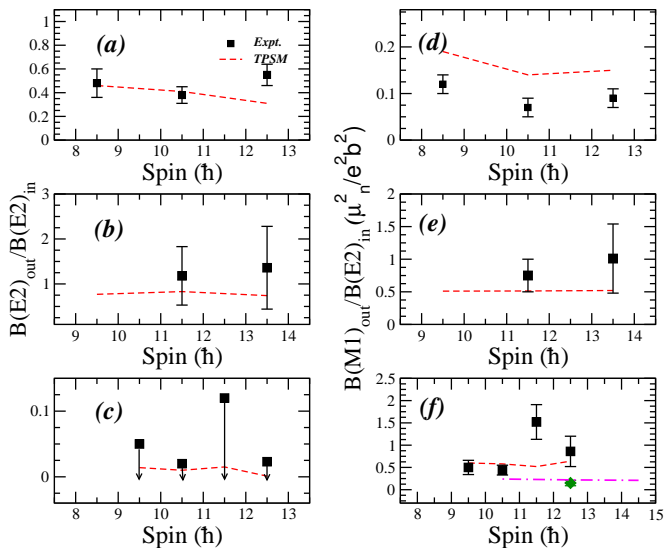


FIG. 4. The ratio of the rates of the out-band $\Delta I = 1$ transitions and the in-band E2 transitions of ^{105}Pd are plotted as a function of spin, I . The E2 and M1 rates for the $\Delta I = 1$ transitions have been estimated using the evaluated values of the mixing ratios (Table I) and are shown on the left and right panels, respectively. The values for the Band 3 \rightarrow Band 1 transitions are shown in (a) and (d), the values for Band 4 \rightarrow Band 2 transitions in (b) and (e), and the values for the Band 3 \rightarrow 4 transition in (c) and (f). Fig. 4(f) also includes the value for the Band 2 \rightarrow Band 1 transition (shown in green), assuming the E2 mixing to be negligible. In Fig. 4(c), the upper bounds correspond to the upper limit of the uncertainties of the mixing ratio values given in Table I. The dotted line on each panel represents the calculated values from TPSM.

The ratios of the inter-band to intra-band transition rates have been plotted in Fig. 4, which show two distinct classes of inter-band $\Delta I = 1$ transitions. In one case, the $B(E2)$ values for these transitions are of the same order as the intra-band $B(E2)$ rates. Thus, these $\Delta I = 1$ transitions from Band 3 to Band 1 and Band 4 to Band 2 (Fig. 4(a) and Fig. 4(b)) have substantial collective enhancement in the $B(E2)$ rates. On the other hand, the $\Delta I = 1$ transitions for Band 3 \rightarrow Band 4 and Band 2 \rightarrow Band 1 are predominantly M1 in nature. The

$B(M1)_{out}/B(E2)_{in}$ values for the $\Delta I = 1$ transitions are plotted in Fig. 4(d), (e) and (f). The ratios for the out-band and in-band transition rates for Band 2 to Band 3 and Band 4 to Band 1 have been plotted in Fig. 5, which shows an increasing trend in the $B(M1)_{out}/B(E2)_{in}$ values for the $\Delta I = 0$ transitions from Band 4 to Band 1 as a function of spin (Fig. 5(b)).

The present analysis establishes that the inter-band $\Delta I = 1$ transitions for Band 2 \rightarrow Band 1 and Band 4 \leftrightarrow Band 3 are predominantly M1, while the $\Delta I = 1$ transitions for Band 3 \rightarrow Band 1 and Band 4 \rightarrow Band 2 shows large enhancement in $B(E2)$ rates.

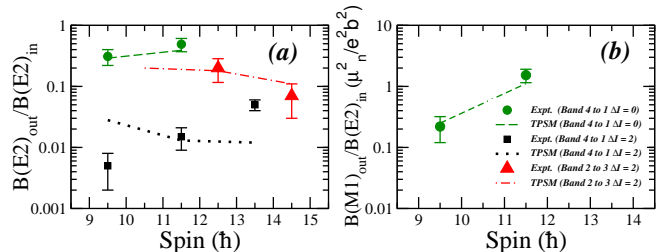


FIG. 5. The ratio of the rates of the out-band $\Delta I = 0$ and $\Delta I = 2$ transitions from Band 4 to Band 1, Band 2 to Band 3 and the in-band E2 transition of Band 4 as a function of spin, I . The M1 and E2 rates have been estimated using the evaluated values of the mixing ratios (Table. I) and plotted in (a) and (b), respectively. The dotted line on each panel represents the calculated values from TPSM.

III. DISCUSSION

To provide an insight into the nature of the band structures observed in ^{105}Pd , triaxial projected shell model (TPSM) [25] calculations have been performed. This model has been shown to provide a unified description of the interplay between collective and single-particle degrees of freedom in deformed odd-mass nuclei [9, 26–28]. In the present study of ^{105}Pd , the deformed basis states have been obtained by solving the triaxial Nilsson potential with $\epsilon = 0.257$ and $\epsilon' = 0.12$ [18]. The monopole pairing interaction is employed by solving standard Bardeen-Cooper-Schrieffer (BCS) equations and the resulting Nilsson + BCS states are then projected onto good angular-momentum states [29]. For odd-neutron nuclei, the basis states are composed of one-neutron and one-neutron coupled to two-proton states, which are sufficient for the discussion of the observed low-lying band structures in ^{105}Pd . We have also evaluated the transition probabilities with the effective charges of 1.6e for protons and 0.6e for neutrons [30–32].

The experimental energies $E(I)$ and the derived rotational frequencies $\hbar\omega(I)$ are compared with the TPSM values in Fig. 7. The calculations reproduce the experimental values for all four bands quite well. The levelling of Band 1 at $\hbar\omega = 0.58$ MeV (“upbend” of the function $I(\omega)$) reflects the rotational alignment of an additional

TABLE II. Transition rates of different bands from TPSM Calculations used for the comparison plots with experimental values.

| Band 2 | | | | |
|---------------------|------------------------------|-------------------------------|--------------------------------|----------|
| Spin (\hbar) | $B(E2)_{in}$ (e^2b^2) | $B(E2)_{out}$ (e^2b^2) | $B(M1)_{out}$ (μ_n^2) | Decay to |
| 10.5 | 0.54 | 0.008 | 0.13 | Band 1 |
| | | | 0.11 | Band 3 |
| 12.5 | 0.82 | 0.008 | 0.18 | Band 1 |
| | | | 0.15 | Band 3 |
| 14.5 | 0.89 | 0.001 | 0.19 | Band 1 |
| | | | 0.09 | Band 3 |

| Band 3 | | | | |
|---------------------|------------------------------|-------------------------------|--------------------------------|----------|
| Spin (\hbar) | $B(E2)_{in}$ (e^2b^2) | $B(E2)_{out}$ (e^2b^2) | $B(M1)_{out}$ (μ_n^2) | Decay to |
| 8.5 | 0.72 | 0.33 | 0.14 | Band 1 |
| | | 0.01 | 0.41 | Band 4 |
| 10.5 | 0.80 | 0.32 | 0.12 | Band 1 |
| | | 0.01 | 0.46 | Band 4 |
| 12.5 | 0.72 | 0.23 | 0.11 | Band 1 |
| | | 0.001 | 0.46 | Band 4 |
| 14.5 | 0.70 | 0.18 | 0.11 | Band 1 |

| Band 4 | | | | |
|---------------------|------------------------------|-------------------------------|--------------------------------|---------------------------|
| Spin (\hbar) | $B(E2)_{in}$ (e^2b^2) | $B(E2)_{out}$ (e^2b^2) | $B(M1)_{out}$ (μ_n^2) | Decay to |
| 7.5 | 0.63 | 0.02 | 0.51 | Band 3 |
| | | 0.23 | 0.08 | Band 1 ($\Delta I = 0$) |
| | | 0.02 | - | Band 1 ($\Delta I = 2$) |
| 9.5 | 0.69 | 0.01 | 0.42 | Band 3 |
| | | 0.53 | 0.35 | Band 2 |
| | | 0.20 | 0.17 | Band 1 ($\Delta I = 0$) |
| 11.5 | 0.72 | 0.02 | - | Band 1 ($\Delta I = 2$) |
| | | 0.01 | 0.38 | Band 3 |
| | | 0.60 | 0.37 | Band 2 |
| 13.5 | 0.74 | 0.28 | 0.79 | Band 1 ($\Delta I = 0$) |
| | | 0.01 | - | Band 1 ($\Delta I = 2$) |
| | | 0.004 | 0.35 | Band 3 |
| | | 0.55 | 0.38 | Band 2 |
| | | 0.27 | 0.65 | Band 1 ($\Delta I = 0$) |
| | | 0.01 | - | Band 1 ($\Delta I = 2$) |

pair of $h_{11/2}$ quasineutrons, which is seen in Fig. 6 as the bands originating from the three-quasineutron configuration at 4.17 MeV become yrast. A similar levelling is found in the TPSM results for Bands 2, 3, and 4 and reflects the crossing of the three-quasineutron configurations. The TPSM levelling is seen in the experimental frequencies of Bands 3 and 4 as well. However, the two experimental frequency points of Band 2 do not confirm the TPSM prediction.

The TPSM wavefunctions have been used to calculate the M1 and E2 transition probabilities between the excited levels of ^{105}Pd , which are listed in Table II. Figs. 4

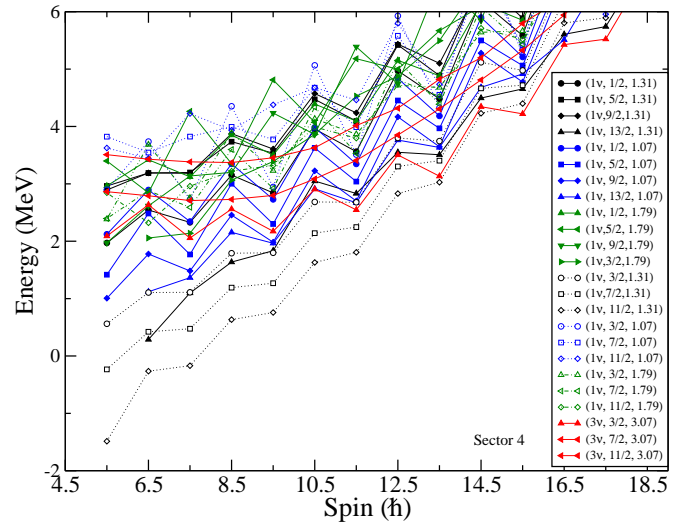


FIG. 6. Energies of the projected K configurations, where the short axis is chosen as the quantization axis 3 to which K refers. The curves are labelled by three quantities: quasiparticle character, K quantum number and energy of the unpaired proton. The legend includes configurations like (1v, 1/2, 1.31), (1v, 5/2, 1.31), (1v, 9/2, 1.31), (1v, 13/2, 1.31), (1v, 1/2, 1.07), (1v, 5/2, 1.07), (1v, 9/2, 1.07), (1v, 13/2, 1.07), (1v, 1/2, 1.79), (1v, 5/2, 1.79), (1v, 9/2, 1.79), (1v, 13/2, 1.79), (1v, 3/2, 1.31), (1v, 7/2, 1.31), (1v, 11/2, 1.31), (1v, 3/2, 1.07), (1v, 7/2, 1.07), (1v, 11/2, 1.07), (1v, 3/2, 1.79), (1v, 7/2, 1.79), (1v, 11/2, 1.79), (3v, 3/2, 3.07), (3v, 7/2, 3.07), and (3v, 11/2, 3.07).

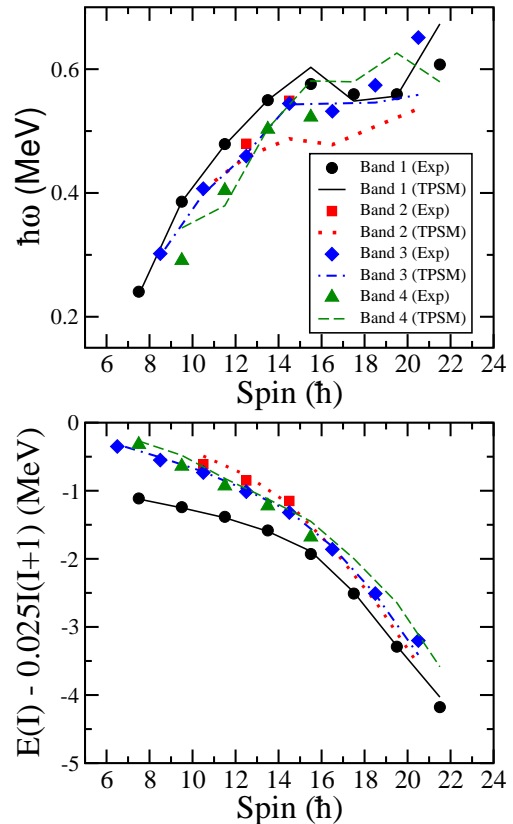


FIG. 7. Experimental and calculated values from TPSM for the rotational frequency (upper panel) and the level energies minus the rotor contribution (lower panel) as functions of the spin I for Bands 1, 2, 3 and 4.

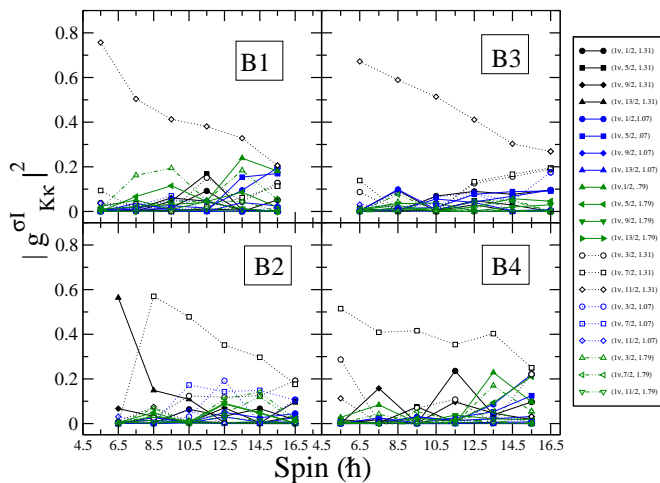


FIG. 8. Probabilities of various projected K configurations in the orthonormal basis shown in Fig. 6. The curves are labelled by three quantities: quasiparticle character, K quantum number and energy of the quasiparticle state. For instance, $[1,1/2,1.31]$ designates one quasineutron state with $K=1/2$ having an intrinsic energy of 1.31 MeV. The symbols and line types agree with Fig.6.

and 5 compare the pertaining ratios with the observed inter-band to intra-band ratios of the transition rates. For all the transitions, the agreement was found to be quite well, which substantiates the suggested interpretation.

The E2 probability for Band 3→Band 1 is enhanced, as expected for collective transition connecting the $n = 1$ TW state with the $n = 0$ yrast state. The transitions Band 2→Band 1 are weak, expected for the SP band, which has a different orientation of the $h_{11/2}$ quasineutron than the yrast band. The transitions Band 4→Band 2 are enhanced, as speculated for the collective E2 transition connecting the $n = 1$ TW excitation on top of the SP states with the SP states. The transitions Band 4→Band 3 are small because the orientation of the $h_{11/2}$ quasineutron differs in the two bands. For the same reason, the transitions Band 4→Band 1 are weak.

In order to further investigate the structure of the observed bands in ^{105}Pd , Fig. 6 shows the energies of the bands projected from the quasiparticle configurations before the TPSM Hamiltonian is diagonalized. It is important to point out that the short principal axis is chosen as the 3-axis of quantization, and “ K ” denotes the angular momentum projection on the short axis. This is different from the TPSM calculations published so far where the long principal axis is chosen as the 3-axis. This choice simplifies the interpretation because, in the TW regime, the odd quasineutron tends to align its angular momentum with the short axis. This has the consequence that the final states are much less mixed with respect to K . Of course, such a change of the quantization axis leaves the observables invariant. Technically, it is achieved by changing the triaxiality parameter γ to an equivalent value in another sector. The

TPSM parameters $\epsilon = 0.257$ and $\epsilon' = 0.12$ correspond to $\epsilon = \epsilon_0 \cos \gamma$ and $\epsilon' = \epsilon_0 \sin \gamma$ with $\epsilon_0 = 0.2795$ and $\gamma = 23.17^\circ$ and the 3-axis being long principal axis. Changing $\gamma \rightarrow -120^\circ - \gamma = -143.172^\circ$ leaves the results invariant but moves the 3-axis to the short principal axis and the corresponding parameters for which the TPSM calculations were performed are $\epsilon = 0.2237$ and $\epsilon' = -0.1675$.

Fig. 8 displays the diagonal components of the K -distribution of the wavefunctions for various angular momentum states for the four observed bands. The lowest sequences of basis states in Fig. 6 are projections from the one-quasineutron configuration at 1.307 MeV onto different values of K . As seen in Fig. 8, for the states $I=11/2, 15/2, 19/2, \dots$ of Band 1 the largest components are the $K=11/2$ states. Decomposing these basis states into their quasineutron factors and collective factors (defined as the projections from the quasiparticle vacuum) shows that the main quasineutron component is $h_{11/2}$ with the projection of the triaxial Nilsson state along the s-axis, $k=11/2$. For the $I=13/2, 17/2, 21/2, \dots$ states of Band 3 band, the same $K=11/2$ basis states appear with the largest probability. The higher energies of the $I=13/2, 17/2, 21/2, \dots$ states compared to the $I=11/2, 15/2, 19/2$, as seen in Fig. 6, are due to a larger fraction of the collective angular momentum. This is the expected structure for the TW mode with the angular momentum of the $h_{11/2}$ quasineutron being aligned with the s-axis.

For $I=17/2, 21/2, \dots$ of band Band 2, the dominating basis state is $K=7/2$ and decomposing it into the quasineutron and collective factors shows that the most probable component is $h_{11/2}$ with the $k=7/2$ projection. It has the characteristic signature partner structure, with the angular momentum of the quasineutron being tilted away from the s-axis. The reorientation of the quasineutron’s angular momentum suppresses the collective E2 transitions Band 2→Band 1 and Band 2→Band 3, and the transitions acquire the M1 character. For the $I=15/2, 19/2, 23/2, \dots$ of Band 4, the largest component is $K=7/2$. The energies of the states are larger as compared to the $13/2, 17/2, 21/2, \dots$, because of the additional collective angular momentum of the wobbling motion. The similar orientation of the quasineutron’s angular momentum allows enhanced E2 Band 4→Band 2 transitions. For Band 4→Band 3 transitions, the change of the quasineutron’s angular momentum alignment with the s-axis suppresses the collective E2 radiation and generates the M1 part.

The above interpretation in terms of the leading basis states loses relevance with increasing I because of the mixing of different K states projected from the quasineutron configuration at 1.307 MeV as well from the configurations at 1.074 MeV and 1.792 MeV. This is reflected by the decrease in the probability of the configuration at 1.307 MeV with increasing I .

The nucleus ^{105}Pd has a structure that is analogous to ^{135}Pr , where the odd $h_{11/2}$ quasineutron replaces the odd quasiprotone. The latter has been studied in Refs.

[5, 6, 17] using the TPSM and the PTR model. Both approaches predict that the second band with the signature $11/2, 15/2, 19/2, \dots$ has the character of the $n=2$ double TW excitation mode, which is in agreement with the strong E2 transition to the $n=1$ single TW band observed in ^{135}Pr [17]. As shown in the present work, this band has a different nature in ^{105}Pd . The TPSM accounts for the different nature of these bands in ^{105}Pd and ^{135}Pr . At variance, the PTR model predicts an $n = 2$ double TW excitations for Band 4 in ^{105}Pd as well [33]. The PTR model predicts the SP band in both nuclei at twice the energy above the yrast band than observed [17, 18], while the TPSM approach reproduces the experimental energy difference quite well. The TPSM takes the antisymmetrization between the odd nucleon and the nucleons of the collective rotor core into account, while the PTR model neglects it. This could be the reason for the discrepancy between the two models.

In summary, the multipolarities and the electromagnetic characters of the gamma transitions from the excited levels of the second band with angular momentum states, $15/2, 19/2, 23/2, \dots$ (Band 4) have been determined through the R_{DCO} and polarization measurements. The transitions connecting it with the previously known single transverse wobbling band (Band 3) are dominated by the M1 component with only weak E2 admixtures. This excludes the interpretation as a double transverse wobbling excitation, which has been suggested for the analogue band in ^{135}Pr . Instead, the band

has been interpreted as a transverse wobbling excitation built on the signature partner band (Band 2). Accordingly, the inter-band $\Delta I = 1$ transitions show large enhancement in the B(E2) rates. Triaxial projected shell model calculations account well for the observed energies and ratios of the transition probabilities. Analyzing the calculated eigenstates, the doublet wobbling nature of the bands observed in ^{105}Pd has been demonstrated.

In comparison to axial nuclei, triaxial systems have the possibility to rotate about the third axis as an additional collective degree of freedom, which generates the wobbling mode as a set of collective excitations. In general, the collective excitations are expected to appear not only based on the yrast band, but also on quasiparticle excitations. The present work identified the first example of such a wobbling mode of a quasineutron excitation - the signature partner band with a transverse wobbling excitation built on it, which is an essential indication of its collective nature.

Private communications on the particle-rotor model results for ^{105}Pd with Prof. Q. B. Chen are gratefully acknowledged. GHB, JAS and NR acknowledge the Science and Engineering Research Board (SERB), Department of Science and Technology, Govt. of India for providing financial support under Project no. CRG/2019/004960 to carry out a part of this research work. AK is thankful to the Council of Scientific & Industrial Research (CSIR), India, for the Senior Research Fellowship vide file no. 09/489(0121)/2019-EMR-I.

-
- [1] P. Möller, R. Bengtsson B. G. Gillis, P. Olivius, T. Ichikawa, *Phys. Rev. Lett.* **97** 162502 (2006).
- [2] A. Bohr and B. R. Mottelson, *Nuclear Structure* (W. A. Benjamin, New York, 1975), Vol. II, Chap. 4.
- [3] S. W. Ødegård, G. B. Hagemann, D. R. Jensen, M. and Bergström, B. Herskind, G. Sletten, S. Törmänen, J. N. Wilson, P. O. Tjøm, I. Hamamoto, K. Spohr, H. Hübel, A. Görge, G. Schönwasser, A. Bracco, S. Leoni, A. Maj, C. M. Petrache, P. Bednarczyk and D. Curien, *Phys. Rev. Lett.* **86**, 5866 (2001).
- [4] R. Bengtsson and H. Ryde, *Eur. Phys. J. A* **22**, 355 (2004).
- [5] S. Frauendorf and F. Dönau, *Phys. Rev. C* **89**, 014322 (2014).
- [6] J. T. Matta, U. Garg, W. Li, S. Frauendorf, A. D. Ayangeakaa, D. Patel, K. W. Schlx, R. Palit, S. Saha, J. Sethi, T. Trivedi, S. S. Ghugre, R. Raut, A. K. Sinha, R. V. F. Janssens, S. Zhu, M. P. Carpenter, T. Lauritsen, D. Seweryniak, C. J. Chiara, F. G. Kondev, D. J. Hartley, C. M. Petrache, S. Mukhopadhyay, D. Vijaya Lakshmi, M. Kumar Raju, P. V. Rao Madhusudhana, S. K. Tandel, S. Ray and F. Dönau, *Phys. Rev. Lett.* **114**, 082501 (2015).
- [7] S. Nandi, G. Mukherjee, Q. B. Chen, S. Frauendorf, R. Banik, Soumik Bhattacharya, Shabir Dar, S. Bhattacharyya, C. Bhattacharya, S. Chatterjee, S. Das, S. Samanta, R. Raut, S. S. Ghugre, S. Rajbanshi, Sajad Ali, H. Pai, Md. A. Asgar, S. Das Gupta, P. Chowdhury and A. Goswami, *Phys. Rev. Lett.* **125**, 132501 (2020).
- [8] S. Chakraborty, H.P. Sharma, S.S. Tiwary, C. Majumder, A.K. Gupta, P. Banerjee, S. Ganguly, S. Rai, Pragati, Mayank, S. Kumar, A. Kumar, R. Palit, S.S. Bhattacharjee, R.P. Singh and S. Muralithar *Phys. Lett. B* **811**, 135854 (2020).
- [9] A. Mukherjee, S. Bhattacharya, T. Trivedi, S. Tiwari, R. P. Singh, S. Muralithar, Yashraj, K. Katre, R. Kumar, R. Palit, S. Chakraborty, S. Jehangir, Nazira Nazir, S. P. Rouoof, G. H. Bhat, J. A. Sheikh, N. Rather, R. Raut, S. S. Ghugre, S. Ali, S. Rajbanshi, S. Nag, S. S. Tiwary, A. Sharma, S. Kumar, S. Yadav and A. K. Jain *Phys. Rev. C* **107**, 054310 (2023).
- [10] D. R. Jensen, G. B. Hagemann, I. Hamamoto, S. W. Ødegård, B. Herskind, G. Sletten, J. N. Wilson, K. Spohr, H. Hübel, P. Bringel, A. Neußer, G. Schönwasser, A. K. Singh, W. C. Ma, H. Amro, A. Bracco, S. Leoni, G. Benzoni, A. Maj, C. M. Petrache, G. Lo Bianco, P. Bednarczyk and D. Curien, *Phys. Rev. Lett.* **89**, 142503 (2002).
- [11] P. Bringel, G. B. Hagemann, H. Hübel, A. Al-khatib, P. Bednarczyk, A. Bürger, D. Curien, G. Gangopadhyay, B. Herskind, D. R. Jensen, D. T. Joss, Th. Kröll, G. Lo Bianco, S. Lunardi, W. C. Ma, N. Nenoff, A. Neußer-Neffgen, C. M. Petrache, G. Schönwasser, J. Simpson, A. K. Singh, N. Singh and G. Sletten, *Eur. Phys. J. A* **24**, 167 (2005).
- [12] G. Schönwasser, H. Hübel, G.B. Hagemann, P. Bednar-

- czyk, G Benzoni, A Bracco, P Bringel, R Chapman, D Curien, J Domscheit, B Herskind, D.R Jensen, S Leoni, G Lo Bianco, W.C Ma, A Maj, A Neußer, S.W Ödegård, C.M Petrache, D Roßbach, H Ryde, K.H Spohr and A.K Singh, *Phys. Lett. B* **552**, 9 (2003).
- [13] H Amro, W.C. Ma, G.B Hagemann, R.M Diamond, J Domscheit, P Fallon, A Görgen, B Herskind, H Hübel, D.R Jensen, Y Li, A.O Macchiavelli, D Roux, G Sletten, J Thompson, D Ward, I Wiedenhöver, J.N Wilson and J.A Winger, *Phys. Lett. B* **553**, 197 (2003).
- [14] D. J. Hartley, R. V. F. Janssens, L. L. Riedinger, M. A. Riley, A. Aguilar, M. P. Carpenter, C. J. Chiara, P. Chowdhury, I. G. Darby, U. Garg, Q. A. Ijaz, F. G. Kondev, S. Lakshmi, T. Lauritsen, A. Ludington, W. C. Ma, E. A. McCutchan, S. Mukhopadhyay, R. Pifer, E. P. Seyfried, I. Stefanescu, S. K. Tandel, U. Tandel, J. R. Vanhoy, X. Wang, S. Zhu, I. Hamamoto and S. Frauendorf, *Phys. Rev. C* **80**, 041304(R) (2009).
- [15] S. Biswas, R. Palit, S. Frauendorf, U. Garg, W. Li, G. H. Bhat, J. A. Sheikh, J. Sethi, S. Saha, Purnima Singh, D. Choudhury, J. T. Matta, A. D. Ayangeakaa, W. A. Dar, V. Singh and S. Sihotra, *Eur. Phys. J. A* **55**, 159 (2019).
- [16] Kosai Tanabe and Kazuko Sugawara-Tanabe *Phys. Rev. C* **95**, 064315 (2017).
- [17] N. Sensharmaa, U. Garg, S.Zhub, A. D. Ayangeakaab, S. Frauendorf, W. Lia, G.H. Bhat, J. A. Sheikh, M. P. Carpenter, Q. B. Chen, J. L. Cozzi, S. S. Ghugre, Y. K. Guptaa, D. J. Hartley, K. B. Howard, R. V. F. Janssens, F. G. Kondev, T. C. McMaken, R. Palit, J. Seth, D. Seweryniak, R. P. Singh, *Phys. Lett. B* **792** 170 (2019).
- [18] J. Timár, Q. B. Chen, B. Kruzsicz, D. Sohler, I. Kuti, S. Q. Zhang, J. Meng, P. Joshi, R. Wadsworth, K. Starosta, A. Algora, P. Bednarczyk, D. Curien, Zs. Dombrádi, G. Duchêne, A. Gizon, J. Gizon, D. G. Jenkins, T. Koike, A. Krasznahorkay, J. Molnár, B. M. Nyakó, E. S. Paul, G. Rainovski, J. N. Scheurer, A. J. Simons, C. Vaman and L. Zolnai, *Phys. Rev. Lett.* **122**, 062501 (2019).
- [19] J. Timár, B. Kruzsicz, I. Kuti, D. Sohler, J. Molnár, B. M. Nyakó, Q.B. Chen, S.Q. Zhang, J. Meng, P. Joshi, R. Wadsworth, K. Starosta and T. Koike *J. Phys.: Conf. Ser.* **1555** 012025 (2020).
- [20] R. Palit, S. Saha, J. Sethi, T. Trivedi, S. Sharma, B. S. Naidu, S. Jadhav, R. Donthi, P. B. Chavan, H. Tan and W. Hennig, *Nucl. Inst. Methods A* **680**, 90 (2012).
- [21] D. C. Radford, *Nucl. Inst. Methods A* **361**, 297 (1995).
- [22] F. A. Rickey, J. A. Grau, L. E. Samuelson and P. C. Simms, *Phys. Rev. C* **15**, 1530 (1977).
- [23] A. Krämer-Flecken, T. Morek, R. Lieder, W. Gast, G. Hebbinghaus, H. Jäger and W. Urban, *Nuclear Instruments and Methods in Physics Research Section A: Accelerators, Spectrometers, Detectors and Associated Equipment* **275**, 333 (1989).
- [24] E. S. Macias, W. D. Ruhter, D. C. Camp and R. G. Lanier *Comp. Phys. Comm.* **11**, 75 (1976).
- [25] J. A. Sheikh and K. Hara, *Phys. Rev. Lett.* **82**, 3968 (1999).
- [26] S. Jehangir, G. H. Bhat, N. Rather, J. A. Sheikh and R. Palit, *Phys. Rev. C* **104**, 044322 (2021).
- [27] J. A. Sheikh, G. H. Bhat, Y. Sun and R. Palit, *Phys. Lett. B* **688**, 305 (2010).
- [28] J. Marcellino, E. H. Wang, C. J. Zachary, J. H. Hamilton, A. V. Ramayya, G. H. Bhat, J. A. Sheikh, A. C. Dai, W. Y. Liang, F. R. Xu, J. K. Hwang, N. T. Brewer, Y. X. Luo, J. O. Rasmussen, S. J. Zhu, G. M. Ter-Akopian and Yu. Ts. Oganessian, *Phys. Rev. C* **96**, 034319 (2017).
- [29] P. Ring and P. Schuck, *The Nuclear Many Body Problem* (Springer-Verlag, New York), (1980).
- [30] G. H. Bhat, W. A. Dar, J. A. Sheikh and Y. Sun, *Phys. Rev. C* **89**, 014328 (2014).
- [31] G. H. Bhat, J. A. Sheikh W. A. Dar, S. Jehangir, R. Palit and P. A. Ganai, *Phys. Lett. B* **738**, 218 (2014).
- [32] G. H. Bhat, R. N. Ali, J. A. Sheikh and R.Palit, *Nucl. Phys. A* **922**, 150 (2014).
- [33] Q. B. Chen, private communication.